MCB
Journals.ASM.org

Endogenous Siderophore 2,5-Dihydroxybenzoic Acid Deficiency Promotes Anemia and Splenic Iron Overload in Mice

Zhuoming Liu, Alieta Ciocea,* L. Devireddy

Case Comprehensive Cancer Center and Department of Pathology, Case Western Reserve University, Cleveland, Ohio, USA

Eukaryotes produce a siderophore-like molecule via a remarkably conserved biosynthetic pathway. 3-OH butyrate dehydrogenase (BDH2), a member of the short-chain dehydrogenase (SDR) family of reductases, catalyzes a rate-limiting step in the biogenesis of the mammalian siderophore 2,5-dihydroxybenzoic acid (2,5-DHBA). Depletion of the mammalian siderophore by inhibiting expression of *bdh2* results in abnormal accumulation of intracellular iron and mitochondrial iron deficiency in cultured mammalian cells, as well as in yeast cells and zebrafish embryos We disrupted murine *bdh2* by homologous recombination to analyze the effect of *bdh2* deletion on erythropoiesis and iron metabolism. *bdh2* null mice developed microcytic anemia and tissue iron overload, especially in the spleen. Exogenous supplementation with 2,5-DHBA alleviates splenic iron overload in *bdh2* null mice. Additionally, *bdh2* null mice exhibit reduced serum iron. Although BDH2 has been proposed to oxidize ketone bodies, we found that BDH2 deficiency did not alter ketone body metabolism *in vivo*. In sum, our findings demonstrate a key role for BDH2 in erythropoiesis.

Erythroid differentiation of hematopoietic stem cells in vertebrates occurs sequentially (1, 2). Unlike other blood cells, mature red blood cells (RBCs) do not have nuclei or organelles. The majority of genes that are important for regulating early stages of differentiation in committed progenitors are effectively silenced during differentiation. In contrast, mechanisms that regulate hemoglobin synthesis are active during the terminal stages of differentiation, which include components of porphyrin synthesis, globin production, and iron acquisition and trafficking (3, 4). These mechanisms ensure that all components are produced stoichiometrically to achieve sustainable hemoglobin production. The importance of regulating porphyrins, globins, and iron in heme biogenesis is highlighted by the fact that deficiencies in these components result in hypochromic and microcytic anemia (5).

Mitochondria are the focal point of iron utilization. Thus, a majority of the iron imported into the cell is utilized in mitochondria for the synthesis of heme and iron-sulfur (Fe-S) clusters. Most studies to date detail cellular uptake of iron and its balance in the cell; however, very little is known about intracellular iron transport pathways. Iron must be shielded and escorted to the sites of utilization in the cell due to its reactivity (6). In an additional step, iron must cross both the outer and inner mitochondrial membranes to the site of heme synthesis, the matrix. Members of the SLC family facilitate iron import into mitochondria. Most notable are SLC25A37, also referred to as mitoferrin 1 (Mfrn1), and SLC25A28, also referred to as mitoferrin 2 (Mfrn2), which are important for mitochondrial iron import into erythroid and nonerythroid cells, respectively (7). ABCB10, a member of the ATP-binding cassette transporter, stabilizes mitoferrin-1 levels in the developing erythron (8).

Heme is synthesized in a series of steps that take place both within and outside mitochondria (reviewed in reference 9). Heme biosynthesis has been extensively studied, and all of the needed enzymes are expressed at high levels during erythroid differentiation. Adequate levels of iron are required to sustain high levels of heme production in developing erythrocytes. Iron is delivered to erythroid precursors via the transferrin (Tf) pathway (4, 5). Iron taken up by this pathway enters the labile iron pool (LIP), which is also referred in the literature as "exchangeable," "regulatory," or "chelatable iron pool" because its identity was established using metal chelators (10–13). The LIP consists of both Fe^{2+} and Fe^{3+} and represents a minor fraction of total cellular iron (~3 to 5%) (14). The LIP links cellular iron uptake with iron utilization, storage in proteins, and export (13, 14). Iron within the LIP is thought to be in steady-state equilibrium and is proposed to bind diverse low-molecular-weight chelaters, such as organic anions (phosphates, citrates, and carboxylates) and polyfunctional ligands (polypeptides and siderophores). Siderophores (from the Greek, meaning "iron carriers" or "iron bearers") are low-molecular-weight, ferric iron-specific chelating agents that are hyperexcreted under low-iron conditions by bacteria and fungi (15). Siderophore-like molecules were also described in eukaryotes, but their identities were unknown (16, 17) until recently (18).

We identified a siderophore-like molecule, 2,5-dihydroxybenzoic acid (2,5-DHBA), in eukaryotes that bears remarkable chemical similarities to the *Escherichia coli* 2,3-DHBA, a bacterial siderophore (18, 19). EntA, an NAD^+-dependent 2,3-dihydro-2,3-dihydrobenzoate dehydrogenase, catalyzes the rate-limiting step in the biosynthesis of 2,3-DHBA. Elimination of EntA completely abolishes the synthesis of 2,3-DHBA (20). BDH2 is a functional homologue of bacterial EntA in eukaryotes that catalyzes an enzymatic reaction leading to the synthesis of 2,5-DHBA. The NAD^+-dependent oxidation of 2,3-diDHBA to 2,3-DHBA requires the catalytic site located in exon 7 (18). A mutation, Tyr144 to Phe144, within the predicted active site completely abrogates

Received 15 February 2014 **Returned for modification** 4 March 2014
Accepted 17 April 2014
Published ahead of print 28 April 2014
Address correspondence to L. Devireddy, lxd59@case.edu.
* Present address: Alieta Ciocea, DeVry University, Seven Hills, Ohio, USA.

doi:10.1128/MCB.00231-14

the enzymatic activity of BDH2 (18). Collectively, these results indicate that BDH2 is a functional homologue of bacterial EntA.

In cultured cells, yeast (*Saccharomyces cerevisiae*), and developing zebrafish embryos, silencing of *bdh2*, which leads to siderophore depletion, results in abnormal accumulation of intracellular iron and heme deficiency (18). The absence of heme in siderophore-depleted cells, yeast, and zebrafish embryos suggests that the siderophore may facilitate mitochondrial iron uptake, although additional mechanisms may exist. Thus, these results suggest that the siderophore is an important regulator of cellular iron metabolism and participates in iron trafficking (18). An alternative to chaperone or siderophore-mediated iron delivery to the mitochondria has been proposed for the developing erythron (21). According to this model, iron is delivered directly into the mitochondria upon contact with Tf-containing endosomes and mitochondria, popularly referred to as the "kiss-and-run" hypothesis (21). This model is based on kinetic and colocalization studies, and consequently the cellular mediators that facilitate this process are unknown.

In the present study, we produced mice lacking exon 7 of the *bdh2* gene by classic homologous recombination to determine the consequences of siderophore depletion on iron metabolism *in vivo*. Homozygous mice are viable, fertile, and produce offspring at the expected Mendelian frequency. However, these mice display iron overload, especially in the spleen, which dissipates over time. The iron overload is exacerbated when the mice are placed on an iron-rich diet, which leads to premature mortality. Contrary to the suggestion that BDH2 plays a role in ketone body metabolism, we found that *bdh2* null mice display unaltered ketone body levels in either a fasted or fed state. The creation of *bdh2* null mice has facilitated probing the role of BDH2 in ketone body oxidation as well as in iron handling.

MATERIALS AND METHODS

Derivation, analysis, and maintenance of *bdh2* null mice. Derivation of *bdh2* null mice is described elsewhere (22). All animal protocols were approved by the Institutional Animal Care and Use Committee of Case Western Reserve University. *bdh2* null mice were maintained on a 129SvimJ genetic background. All experiments were performed using age- and gender-matched control mice. Unless indicated, animals were maintained on a standard laboratory diet (Prolab RMH3000 containing 0.02% [wt/wt] iron; LabDiet).

Iron diet studies. Adult mice (8 to 10 weeks old) were placed on a low-iron diet (TD.80396, containing 0.0006% [wt/wt] iron and 0.001% [wt/wt] ethoxyquin) or high-iron diet (TD.08496, containing 2% [wt/wt] carbonyl iron and 0.001% [wt/wt] ethoxyquin). Both diets were custom formulated by Harlan-Teklad (Madison, WI). Mice were kept on iron-manipulated diets for indicated periods of time.

Metabolite measurements in plasma. Plasma samples from wild type (wt) and *bdh2* null mice were analyzed for D-β-OH butyric acid and acetoacetate at the Marshfield Labs (Marshfield, WI).

Hematological parameters. Heparinized blood was obtained by retro-orbital or tail vein phlebotomy. Red blood cell (RBC) count, hemoglobin, hematocrit, and mean corpuscular volume were determined using a Hemavet machine (Drew Scientific). Wright-Giemsa (Dade Behring)-stained peripheral blood smears were photographed using an Olympus microscope with a 100× oil immersion lens.

Serum and iron measurements. Whole blood was collected by terminal bleeding. Nonhemolyzed serum was collected and analyzed for total iron and transferrin saturation using a serum iron/total iron-binding capacity (TIBC) kit from Sigma as per the manufacturer's instructions.

Hematofluorometry. Whole blood from wt and *bdh2* null mice was collected and checked for clots. Blood cells were separated from plasma by centrifugation at 800 × *g* for 5 min at 4°C. Plasma was removed, and the cell pellet was washed three times with phosphate-buffered saline (PBS) to remove interfering pigments. Washed RBCs were then resuspended in PBS, and the whole-blood Zn protoporphyrin/heme (ZnPP/H) ratio was determined using a hematofluorometer as described previously (23).

Quantification of heme biosynthesis. (i) Labeling of apo-Tf. We labeled Tf by following the procedure described in references 7 and 24. Briefly, $^{55}FeCl_3$ was mixed with 0.1 M nitrilotriacetic acid (NTA) to fully chelate iron. The ^{55}Fe-NTA mixture was incubated with apo-transferrin (apo-Tf) (Sigma) until the solution turned pink. We purified the ^{55}Fe-Tf over PD-10 desalting columns (Pharmacia) and determined the concentration of ^{55}Fe-Tf in the eluted material by spectrometry at A_{280}. The specific activity of ^{55}Fe-Tf was determined by the formula specific activity = total cpm/pmol of estimated apo-Tf from A_{280} readings. This procedure typically yields ~10^3 cpm/pmol of Tf.

(ii) Derivation of immortalized hematopoietic cells. *bdh2* null embryonic stem (ES) cells were obtained from Case Western Reserve University Transgenic and Targeting Core Facility and cultivated using ES-Cult maintenance kit from Stem Cell Technologies (Vancouver, BC, Canada). ES cells were differentiated *in vitro* to form hematopoietic progenitors using the ES-Cult hematopoietic progenitor kit from Stem Cell Technologies as per the manufacturer's instructions. Erythroid colonies were identified as per the guidelines set forth by the manufacturer. Disaggregated erythroid colonies were immortalized by cocultivation with irradiated NIH 3T3 TLX1 producer cells in an infection medium (Iscove's modified Dulbecco's medium [IMDM] plus 15% fetal bovine serum [FBS], 100 U/ml penicillin-streptomycin, 2 mM glutamine, 10 ng/ml interleukin-3 [IL-3], 2 ng/ml IL-6, 5 ng/ml IL-11, 50 ng/ml c-kit ligand) for 5 days (25).

(iii) Labeling of cells with ^{55}Fe-Tf. Cells growing in suspension were collected and metabolically labeled with ^{55}Fe-Tf and 0.2 mM 5-aminolevulinic acid (ALA) (Sigma). Briefly, cells were starved of iron by culturing in serum free IMDM for 1 h at 37°C. Cells were washed and recultured in IMDM containing 10% dialyzed FBS (Invitrogen), 0.2 mM ALA, and 2.5 μM ^{55}Fe-Tf for an additional 8 h at 37°C (also see reference 7). Labeled cells were washed with PBS and lysed in a mixture containing 25 mM HEPES (pH 7.8), 1% Triton X-100, and 1% sodium deoxycholate. Genomic DNA was sheared by repeated passage through a 25-gauge needle fitted onto a 1-ml syringe. The cell lysate was then centrifuged at 10,000 rpm at 4°C, and the supernatant was transferred into a fresh tube. A portion of the lysate (~10 μl) was used to determine the total iron concentration. Heme was then extracted by mixing equal amounts of lysate with ethyl acetate and acetic acid mixture, and the organic phase was extracted. Radioactivity in the extracted phase was then determined by liquid scintillation. Nonheme iron was calculated as the difference between total cellular iron and heme iron.

Iron uptake measurements in reticulocytes. Reticulocytosis was induced in wt and *bdh2* null mice by serial phlebotomy on days 0 and 3. Mice were terminally bled on day 7, and the whole blood was collected into heparinized tubes. After 3 washes with ice-cold PBS, reticulocytes (as judged by new methylene blue staining) were counted in a hemocytometer. Cells were resuspended in Hanks' balanced salt solution (HBSS) containing 1% bovine serum albumin (BSA). For iron uptake experiments, reticulocytes were incubated with 3.75 μM ^{55}Fe-Tf for 0 min and 30 min. Zero-time samples were obtained by adding ice-cold ^{55}Fe-Tf to reticulocytes incubated on ice. Total iron and heme iron concentrations were determined as described above.

Tissue iron measurements. Nonheme iron in parenchymal tissues was determined in a colorimetric assay as described previously (18, 26). Briefly, 50 mg of dried tissue was incubated with acid buffer at 65°C for 48 h. The supernatants were collected by centrifugation at 10,000 × *g* for 5 min and treated with iron detection reagent, and the change in absorbance was measured at 560 nm. A standard curve was determined using a solu-

tion containing increasing amounts of iron (Fluka). Tissue iron content was determined by comparing the absorbance values against an iron standard.

AA spectroscopy. Iron content in parenchymal tissues was determined by atomic absorption (AA) spectroscopy. Briefly, 50 mg of dried tissue was incubated in acid digestion buffer (37% HCl, 3% trichloroacetic acid) at 65°C for 18 h. Acid-treated samples were then diluted with iron-free water. Samples were analyzed by flame atomic absorption spectroscopy to determine the iron ion concentration. A standard curve was determined using a solution containing increasing amounts of iron (Fluka). Tissue iron content was determined by comparing the absorbance values against an iron standard.

Mitochondrial enzyme assays. Mitochondria were isolated from 3- and 14-month-old female mouse liver homogenates by differential centrifugation as described in reference 27. The protein concentration was determined by the Bradford method (Bio-Rad). The suspension was stored frozen at −80°C. Mitochondrial aconitase (mAco) was determined as previously described (18) using an extinction coefficient of 1.8 mM^{-1} cm^{-1}. Citrate synthase activity was assayed as previously described (18) using an extinction coefficient of 6.8 mM^{-1} cm^{-1}.

Determination of SDH levels in mouse sera. Serum samples were obtained by phlebotomy of the saphenous vein. Sorbitol dehydrogenase (SDH) levels in serum samples from mice placed on normal chow and a high-iron diet were determined using an enzyme-linked immunosorbent assay (ELISA) kit from Mybiosource following the manufacturer's instructions. Values are presented in units/liter.

Cell culture. 293T cells (ATCC) were cultured in Dulbecco's modified Eagle's medium (DMEM) supplemented with 10% fetal bovine serum, 100 U/ml penicillin, and 100 μg/ml streptomycin. 293T cells were transfected with Lipofectamine (Invitrogen) as per the manufacturer's protocol.

Immunoblot analysis. Minced liver and spleen samples from wt and *bdh2* null mice were homogenized in cold PBS and pelleted at 1,000 × *g*, and the protein concentration in the supernatant was determined using the bicinchoninic acid (BCA) protein assay kit (Pierce). As a positive control for the experiments, we also analyzed lysates from 293T cells transfected with pCMV6 containing the c-*Myc*-tagged full-length mouse *FPN1* cDNA (Origene). Samples were mixed with SDS-Laemmli buffer without heating, and proteins were electrophoretically separated along with molecular weight standards (Invitrogen) on discontinuous SDS-PAGE gels. The protein was transferred onto a nitrocellulose membrane (Bio-Rad). The blot was probed with an antiferroportin antibody (Alpha Diagnostics). The blot was stripped and reprobed with antiactin antibody (Sigma) to verify equal loading.

Histological procedures. Liver and spleen samples were fixed in 10% buffered formalin and embedded in paraffin. Deparaffinized tissue sections were stained with the Perls Prussian blue stain for nonheme iron. Nonheme iron stains blue. Hematoxylin and eosin (H&E) staining was performed using a kit from Sigma as per the manufacturer's procedure.

RNA isolation and gene expression analysis. Total RNA was isolated from liver samples by the TRIzol method (Invitrogen). DNase I (Promega)-treated RNA was reverse transcribed using Superscript III reverse transcriptase (RT) from Invitrogen as per the manufacturer's recommendations. The resulting cDNAs were used for real-time PCR analysis using SYBR green master mix (Promega) following the manufacturer's recommendations. The fold change was calculated by the cycle threshold ($\Delta\Delta C_T$) method.

Statistical analysis. Statistical analysis was performed using JMP statistical software. Data are represented as means ± standard deviations (SD). Two-tailed Student's *t* test was applied for comparisons of two groups, and Welch's correction was applied for unequal variance. One-way analysis of variance followed by the Tukey honestly significant difference (HSD) was applied for multiple comparisons. Survival was evaluated by the Kaplan-Meier log rank test. For all tests, a P value <0.05 was considered significant.

RESULTS

Targeted disruption of the murine *bdh2* gene. Our previous studies indicated that BDH2 catalyzes the biogenesis of 2,5-DHBA, a component of the mammalian siderophore. Depletion of 2,5-DHBA alters intracellular iron homeostasis and results in mitochondrial iron deficiency in cultured cells, yeast, and developing zebrafish embryos (18). This study indicated the need to study BDH2 in iron homeostasis under normal physiological conditions and in disease through the creation of genetically altered mice. Therefore, mice were generated that lack BDH2 by standard genetic manipulation. The catalytic activity of BDH2 depends on the NPG motif encoded in exon 7 (18, 28). Additionally, amino acid sequences encoded by exon 7 of *bdh2* form a helix that is located at a dimer interface within the tetramer (Fig. 1B) (28); removal of these helices prevents proper dimer/tetramer formation. In addition, this helical stretch contains 3 amino acids that form the active site: Tyr147 and Lys151 residues, which are critical for interaction with NAD^+ cofactor, and Arg144, which interacts with a sulfate, lie within this helix (Fig. 1B) (28). Mutation of this region abolishes the enzymatic activity of BDH2 and consequently abrogates the biogenesis of 2,5-DHBA (18). Therefore, to abolish BDH2 activity, exon 7 of the *bdh2* gene was replaced with a neomycin resistance cassette (Fig. 1A) (22). Homologous recombination was confirmed using DNA samples from clones resistant to both G418 and ganciclovir by Southern blotting of HindIII- or EcoRI-digested DNA using 5′ and 3′ probes (Fig. 1C). Chimeric animals were bred with 129SvimJ females to produce inbred F1 offspring carrying the modified *bdh2* allele. We confirmed the germ line transmission of the targeted allele by Southern blotting and PCR analysis (Fig. 1D) (unpublished data). We obtained nearly 25% *bdh2* null mice in F2, suggesting that *bdh2* deletion did not reduce the viability of the embryos. The *bdh2* null mice are grossly indistinguishable from their normal counterparts when maintained on a basal-iron diet (0.02% iron); no overt neurological or developmental abnormalities were observed on this diet.

Bdh2 null mice have no detectable 2,5-DHBA. We previously demonstrated that suppression of BDH2 results in depletion of 2,5-DHBA in cultured mammalian cells (18). We next determined 2,5-DHBA levels in *bdh2* null mice. Salicylic acid derivatives such as 2,5-DHBA are easily detectable in urine specimens (29). Therefore, we analyzed 2,5-DHBA levels in urine samples collected from wt and *bdh2* null mice by gas chromatography-mass spectrometry (GC-MS) analysis following derivatization with trimethylsilate (TMS) (18). We readily observed 2,5-DHBA in the urine samples obtained from wt mice, which was confirmed against a set of DHBA standards. In contrast, there was no detectable 2,5-DHBA in urine samples obtained from *bdh2* null mice (22). Thus, these results not only confirm our previous findings (18) but also reinforce the notion that BDH2 catalyzes the biosynthesis of 2,5-DHBA.

Complete blood counts in 2,5-DHBA-deficient mice. Depletion of siderophore in developing zebrafish embryos results in anemia and heme deficiency (18). We next evaluated hematological parameters in our *bdh2* null mice. Examination of complete blood counts (CBC) and red blood cell (RBC) indices in peripheral blood of *bdh2* null mice (ages 3 to 14 months) revealed a few changes. We found that adult, but not geriatric, *bdh2* null mice were mildly anemic, as noted by a decreased mean corpuscular volume (MCV) (Fig. 2C) and decreased mean corpuscular hemo-

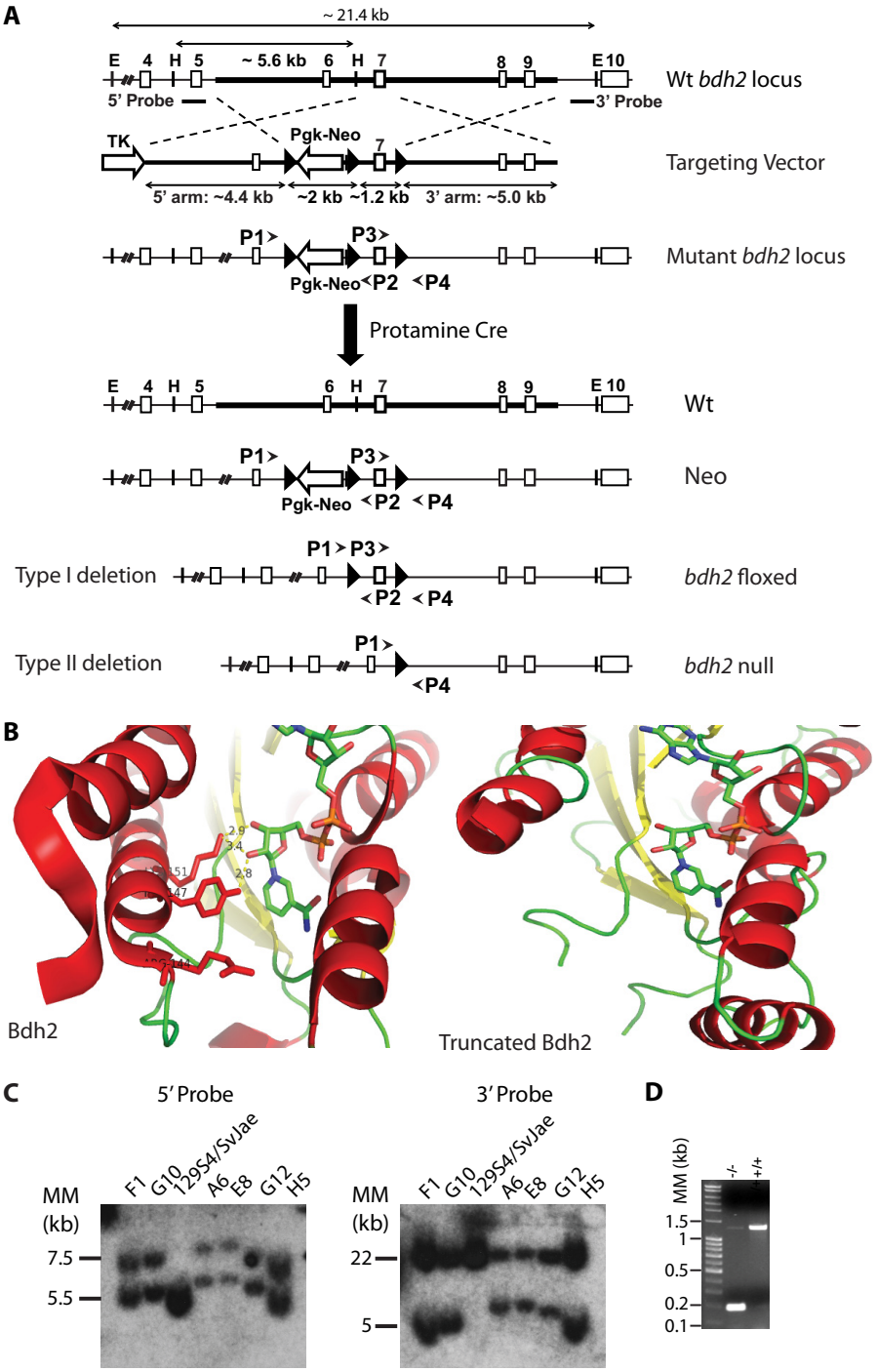

FIG 1 Derivation of *bdh2* knockout mice. (A) Targeting strategy to delete exon 7 in the mouse *bdh2* gene. TK, thymidine kinase. (B) Ribbon diagrams of wt and mutant mouse Bdh2 proteins with bound NAD^+ in a stick model. Note that Tyr147 and Lys151, the critical residues for interaction with NAD^+, are absent in mutant Bdh2. (C) Identification of positive ES clones by Southern blotting using both 5′ and 3′ external probes. (Left) Homologous recombination at the 5′ end. Two clones contained the expected 7.5-kb HindIII fragment with the 5′ external probe. (Right) Homologous recombination at the 3′ end. Two clones, which were targeted correctly at the 5′ end, were tested for targeting at the 3′ end. These clones contained the expected 22-kb EcoRI fragment with the 3′ external probe. (D) Genotype identification by PCR analysis. DNA extracted from tails of wt and *bdh2* type II mice was subjected to PCR analysis. The diagnostic product for type II deletion is the 160-bp fragment amplified by the P1 and P4 primers. MM, molecular marker 1-kb DNA ladder.

globin concentration (MCHC [Hgb/RBC]) (Fig. 2D). Additionally, analysis of peripheral blood smears indicated a mild hypochromia (Fig. 2G). Based on these results, we conclude that *bdh2* null mice are microcytic and hypochromic. These observations are consistent with our previous findings that siderophore-depleted zebrafish embryos were hypochromic (17). Additionally, adult *bdh2* null mice, but not geriatric mice, have a higher number of RBCs than wt controls (Fig. 2A). These results are consistent

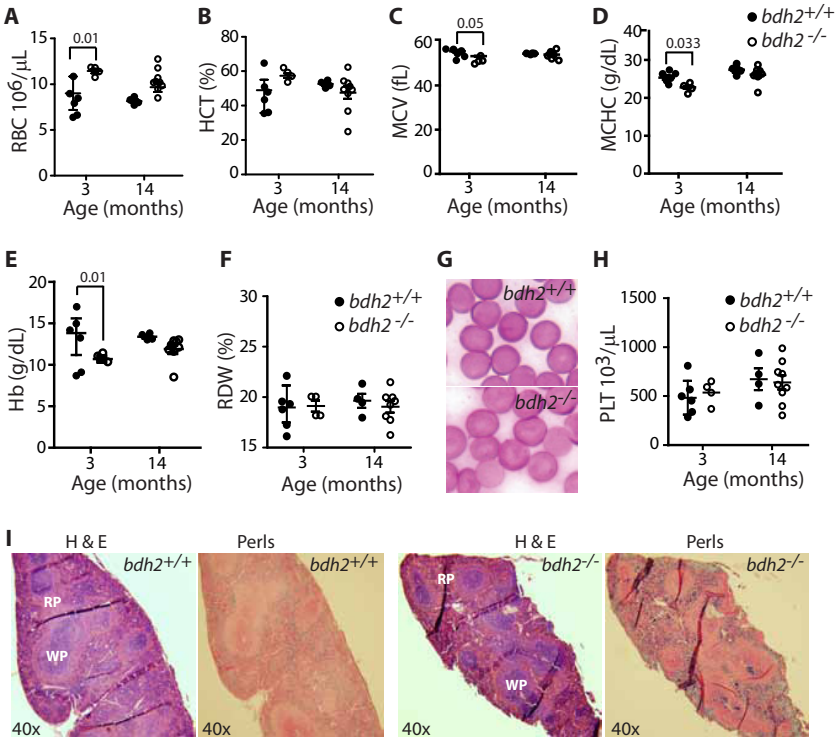

FIG 2 Effect of BDH2 deficiency on hematological parameters. Complete blood counts were measured from whole blood of mice at the indicated ages. (A to F) RBC parameters were determined in female mice at 3 and 14 months of age. Data are presented as means ± SD. HCT, hematocrit; MCV, mean corpuscular volume; MCHC, mean corpuscular hemoglobin concentration; Hb, hemoglobin; RDW, red cell distribution width. (G) Wright-Giemsa-stained peripheral blood smears of mice at 3 months of age. *bdh2* null RBCs are relatively hypochromic. (H) Platelet (PLT) levels in female mice at 3 and 14 months of age. Data are presented as means ± SD. (I) Increased extramedullary hematopoiesis in *bdh2* null mice. Shown are H&E staining and Perls staining of histological sections of spleen from female mice at 14 months of age. WP, white pulp; RP, red pulp.

with the notion that mice with microcytic and hypochromic anemias have a higher number of RBCs (30–32). The increased number of RBCs with a decrease in size further suggests that the iron available for hemoglobin is restricted (30). Despite the presence of mild anemia in *bdh2* null mice, we did not observe splenomegaly, although there was a trend toward increased erythropoiesis on histological examination (Fig. 2I) (unpublished data). No differences in white blood cell (WBC) counts or platelet numbers were detected in *bdh2* null mice (Fig. 2H) (unpublished data). Thus, the results confirm our previous findings and suggest that siderophore depletion affects heme biogenesis.

Mammalian siderophore 2,5-DHBA deficiency causes iron overload. Previously we demonstrated that depletion of 2,5-DHBA through inhibition of *bdh2* expression alters cellular iron homeostasis (18). To assess the consequences of the BDH2 deficiency on iron homeostasis in various organs, we used both histological staining and quantitative determination of iron content (Fig. 3). At 3 months of age, *bdh2* null mice showed a significant increase in iron content in the spleen (~3-fold), which primarily reflects macrophage iron content recovered from the hemoglobin of senescent RBCs (Fig. 3B). We next examined sites of iron accumulation by staining histological sections for iron. We found enhanced iron accumulation in the red pulp region of the spleen (Fig. 3A). However, the histological appearance of the spleen remains unchanged compared to that of wt mice, as judged by H&E staining (Fig. 3A). Siderophore depletion elevates cytoplasmic iron and mitochondrial iron deficiency (18). Thus, the observed increase in splenic iron content may be secondary due to delayed iron utilization in the absence of siderophore.

We also examined the iron content of the liver in 3- and 14-month-old *bdh2* null mice, which reflects total body iron stores. We observed a moderate increase in nonheme iron in liver (~2-fold) in *bdh2* null mice (Fig. 3C). The observed increase in iron content in liver is pronounced in parenchymal cells (Fig. 3A). However, the iron content in the pancreas, heart, and brain of *bdh2* null mice is unremarkable (Fig. 3D and E). The increased iron content observed in spleen and liver samples from 3-month-old *bdh2* null mice is not a permanent change, since analysis of iron content in samples from geriatric wt or *bdh2* null mice (14 months of age) showed no significant difference in iron content (Fig. 3B and C). These findings indicate that *bdh2* deficiency in mice leads to iron accumulation in spleen and, to a more limited extent, in liver.

Finally, analysis of serum iron in *bdh2* null mice revealed a decrease in serum iron and transferrin saturation compared to the levels in wt mice (Fig. 3F and G).

Hepcidin and ferroportin levels are normal in *bdh2* null mice. Hepcidin regulates systemic iron by controlling duodenal iron absorption and release of iron from splenic macrophages (33). Since *bdh2* null mice specifically accumulate iron in the spleen, we reasoned that enhanced iron in spleen might be secondary to altered hepcidin levels. To examine this idea, we assessed levels of hepcidin in liver samples from wt and *bdh2* null mice. Figure 4A shows that there is no significant difference in levels of

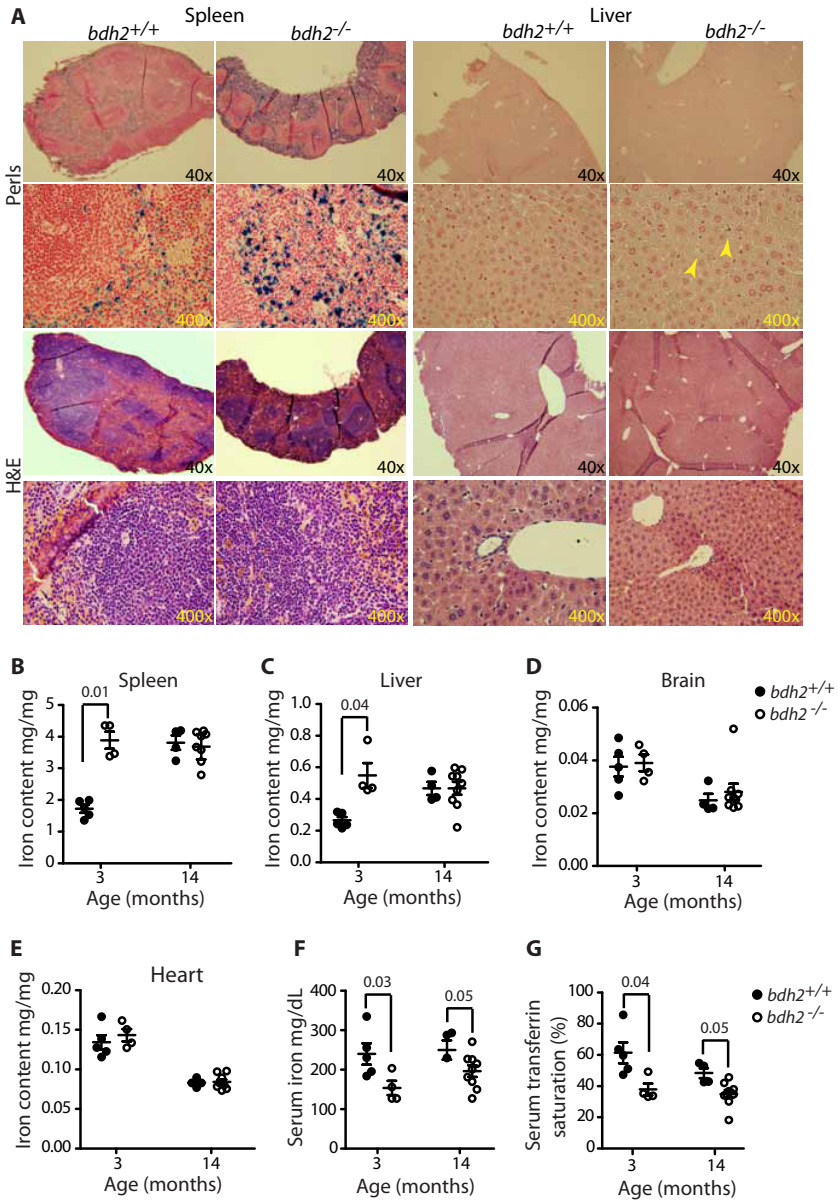

FIG 3 Iron accumulation in *bdh2* null mice. (A) Histological detection of tissue iron in liver and spleen sections from female mice at 14 months of age by Perls or H&E staining. Blue staining represents iron accumulation in cells. Representative images from specimens collected from at least 3 mice per genotype are shown. (B to E) Quantitative determination of tissue iron content (mg/g of tissue wet weight) in various organs was compared in female mice at 3 and 14 months of age. At least 3 mice per time point and genotype were analyzed. Data are presented as means ± SD. (F and G) Serum iron indices in female mice at 3 and 14 months of age. Iron and transferrin saturation were measured from nonhemolyzed serum of wt and *bdh2* null mice. Data are presented as means ± SD.

hepcidin gene expression between wt and *bdh2* null liver samples in aged mice. However, we did observe a trend toward increased hepcidin expression in liver samples from *bdh2* null mice at 12 weeks of age, but the difference did not achieve statistical significance ($P = 0.12$).

Hepcidin binds to ferroportin on the plasma membrane of enterocytes, macrophages, hepatocytes, and other cells, promoting its internalization and eventually lysosomal degradation (34, 35). Ferroportin is the only exporter of inorganic iron in mammalian cells; therefore, inactivation of ferroportin by hepcidin leads to intracellular iron retention (34). We therefore assessed levels of ferroportin by performing an immunoblot of liver and spleen samples from control and *bdh2* null mice. We found that ferroportin levels are similar in both sets of mice (Fig. 4C). Taken together, the results of Fig. 4A and C suggest that hepcidin and ferroportin levels are unaffected by BDH2 deficiency.

Mammalian siderophore 2,5-DHBA depletion confers mitochondrial iron deficiency. The ratio of erythrocyte zinc protoporphyrin IX to heme (ZnPP/H) is commonly used to determine whether iron scarcity affects heme biosynthesis (23, 31, 32). Chelation of iron to protoporphyrin by ferrochelatase is the final step in heme biogenesis. Zn is the alternative metal used by ferrochelatase when iron is not available (36). Therefore, iron deficiency resulting from excess hemolysis and defects in iron recycling con-

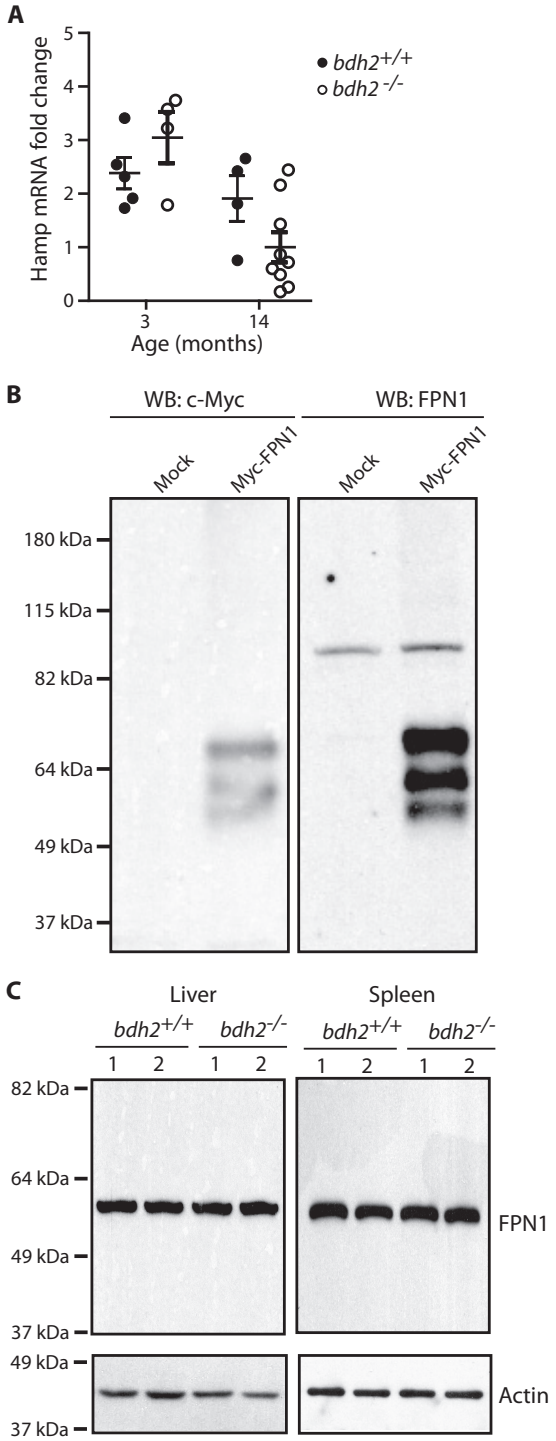

FIG 4 Hepcidin and ferroportin levels are unaltered in *bdh2* null mice. (A) Quantification of hepcidin mRNA levels in liver samples from control and *bdh2* null mice. Shown is hepatic *Hamp* mRNA expression relative to β-actin mRNA expression in control and *bdh2* null mice at 3 months of age. Data are presented as means ± SD. The *P* value is not significant compared with control mice. (B and C) Immunoblot (Western blot [WB]) analysis of ferroportin levels in liver and spleen samples from female mice 3 months of age. Protein samples were collected from mouse liver and spleen homogenates or 293T cells transfected with pCMV6 vector (Origene) or pCMV6 containing c-*Myc*-tagged full-length mouse *FPN1* cDNA. (B) (Left) The blot was probed with anti c-Myc antibody. (Right) The blot was probed with antiferroportin antibody. (C) The blot was probed with antiferroportin antibody. The blot was later stripped and reprobed with an antiactin antibody to ensure equal loading. The positions and masses of molecular mass markers are indicated on the left.

tribute to an increase in the ZnPP/H ratio (31, 32). Yeast and zebrafish embryos deprived of siderophore display mitochondrial iron deficiency (18). Therefore, the ZnPP/H ratio was determined in whole-blood samples from wt and *bdh2* null mice by hematofluorometry (23). The ZnPP/H ratio was increased in *bdh2* null mice (Fig. 5A).

We next measured heme in immortalized hematopoietic cells by labeling them with ^{55}Fe-transferrin and the heme precursor aminolevulinic acid (ALA) (7). As expected, wt cells efficiently incorporated ^{55}Fe into heme; however, in contrast, incorporation of ^{55}Fe into heme was significantly reduced in *bdh2* null hematopoietic cells (Fig. 5B). Finally, we measured incorporation of iron into heme in isolated reticulocytes from wt and *bdh2* null mice. Reticulocytes from serially phlebotomized mice were incubated with ^{55}Fe-Tf (7), and the amount of intracellular iron incorporated into heme was measured. Iron incorporation into heme was lower in reticulocytes from *bdh2* null mice (Fig. 5C).

To further explore mitochondrial iron deficiency, we measured the activity of mitochondrial aconitase (mAco), an iron-dependent enzyme, in liver samples from control and *bdh2* null mice at 3 and 14 months of age (18). We found that mAco activity was substantially lower in liver from *bdh2* null mice (Fig. 5D). In contrast, the activity of citrate synthase (CS), the activity of which is not dependent on iron, is unaltered in *bdh2* null mice (Fig. 5D).

Mammalian siderophore 2,5-DHBA-deficient mice are sensitive to iron challenge. To investigate whether iron deposition in spleen was due to an intrinsic capacity of *bdh2* null mice to load iron, 8-week-old control and *bdh2* null mice were placed on iron-manipulated diets: a low-iron diet (0.0006% iron), a basal-iron diet (0.02% iron), and a high-iron diet (2% carbonyl iron) for 60 days. All control mice regardless of iron content in the diet survived for the duration of the experiment, whereas only 20% of *bdh2* null mice were viable at 55 days post-high-iron-diet challenge (Fig. 6). In contrast, iron deficiency did not cause mortality in *bdh2* null mice, which exhibited pale paws, extreme alopecia, and hypothermia (Fig. 6A). *bdh2* null mice on the high-iron diet exhibited runted growth (Fig. 6A) and gained weight very slowly (Fig. 6). The observed delay in weight gain was unrelated to consumption of chow; both wt and *bdh2* null mice consumed chow at comparable rates (unpublished data).

To gain insight into the mechanism by which a high-iron diet kills *bdh2* null mice, we systematically examined the biochemical and organ changes in these mice. We first evaluated the effect of dietary iron on hematological parameters in wt and *bdh2* null mice. RBCs are elevated in both genotypes on a high-iron diet compared with RBCs in mice on the basal-iron diet or low-iron diet. However, the hemoglobin and MCH contents are significantly lower in *bdh2* null mice, even on the high-iron diet, confirming that 2,5-DHBA deficiency results in heme deficiency (Table 1). Additionally, the MCV is also lower in *bdh2* null mice, suggesting the development of microcytic hypochromic anemia, even in the face of excess iron (Table 1). In contrast, both wt and *bdh2* null mice are anemic when maintained on a low-iron diet (Table 1).

We next examined tissue and serum iron levels in these mice. We found a significant increase in total serum iron and transferrin

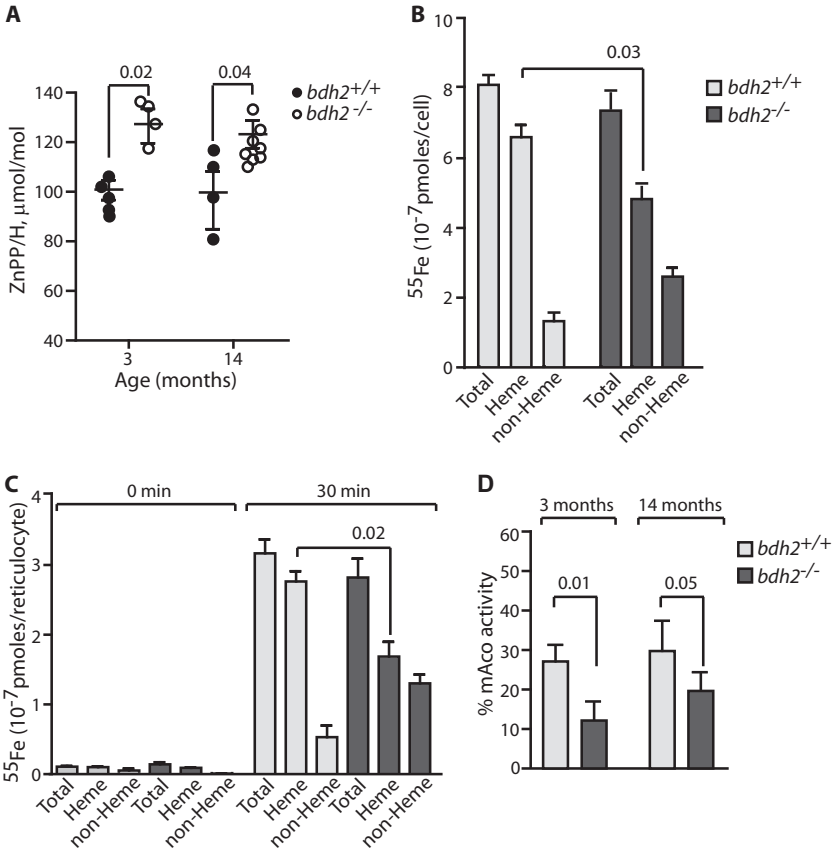

FIG 5 Mitochondrial iron deficiency in hematopoietic cells from *bdh2* null mice. (A) Evaluation of ZnPP/H levels in RBC from control and *bdh2* null mice at 3 months of age. Data are presented as means ± SD. (B) BDH2 deficiency impairs heme biosynthesis in hematopoietic cells. Control or *bdh2* null immortalized hematopoietic cells were incubated with 2.5 μM ^{55}Fe-Tf and 0.2 mM ALA for 8 h at 37°C. Radiolabeled heme was quantified by liquid scintillation following extraction from cell lysates. Data are presented as means ± SD. (C) Incorporation of ^{55}Fe into reticulocytes from control or *bdh2* null mice. Shown are uptake of ^{55}Fe and the distribution of iron between heme and nonheme portions of cellular iron. Reticulocytes were incubated with 3.75 μM ^{55}Fe-Tf at 37°C for 30 min. Time zero values were obtained by incubating ice-cold ^{55}Fe-Tf with reticulocytes on ice. (D) Activity of mitochondrial aconitase (mAco; nmol/min/mg protein) was measured in mitochondria isolated from liver samples from female control and *bdh2* null mice at 3 and 14 months of age. The activity of mAco was normalized to citrate synthase (CS) activity determined from the same samples. The percentage of mAco activity is indicated (mAco/CS × 100). Each value represents the mean ± SD of $n = 5$/genotype.

saturation in both wt and *bdh2* null mice that were kept on a high-iron diet. However, serum iron levels in *bdh2* null mice were much higher than those of wt mice on high-iron diets (Fig. 7A and B). In contrast to these findings, maintenance on a low-iron diet produced lower serum iron levels and decreased transferrin saturation in both groups of mice (Fig. 7A and B). Furthermore, the serum iron levels in mice on a low-iron diet were not significantly different between genotypes (Fig. 7A and B). Dietary carbonyl iron overload is associated with deposition of iron in periportal hepatocytes (37). Thus, we also found enhanced iron staining in periportal areas in control and *bdh2* null mice (Fig. 7C). Additionally, iron accumulation in the liver of *bdh2* null mice was significantly greater than that in liver samples from control mice (Fig. 7C). To confirm these findings, liver iron content was quantified by atomic absorption (AA) spectroscopy and colorimetry. Again, liver iron content was significantly higher in *bdh2* null mice (Fig. 7D and E).

We previously showed that BDH2 deficiency leads to abnormal accumulation of iron in the cytoplasm, leading to increased reactive oxygen species (ROS) production, which eventually contributes to premature cell death (18). Thus, it is possible that iron-loaded hepatocytes in *bdh2* null mice undergo premature cell death. To investigate this possibility *in vivo*, we assessed hepatocyte cell injury by measuring serum levels of sorbitol dehydrogenase (SDH), a liver-specific intracellular enzyme that leaks into blood following hepatic damage (38). We found an ~50-fold increase in serum SDH levels in *bdh2* null mice placed on a high-iron diet over the level found in control mice on the same diet (Fig. 7G). In contrast to the findings observed with the high-iron diet, the low-iron diet significantly lowered liver iron content, as determined using histological and quantitative assays (Fig. 7D and E). Combined, these results suggest that the absence of *bdh2* exacerbates iron accumulation when mice are challenged with excess iron.

Last, we evaluated the iron content in spleens of wt and *bdh2* null mice that were fed a high-iron diet. Figure 3 demonstrates that *bdh2* deficiency contributes to iron accumulation in the spleen. Iron accumulation in the spleen was further exacerbated when *bdh2* null mice were placed on a high-iron diet (Fig. 7C). AA spectrometry and colorimetric determination of iron content confirmed the histological findings in both control and *bdh2* null mice (Fig. 7F) (unpublished data). In contrast to these findings, a

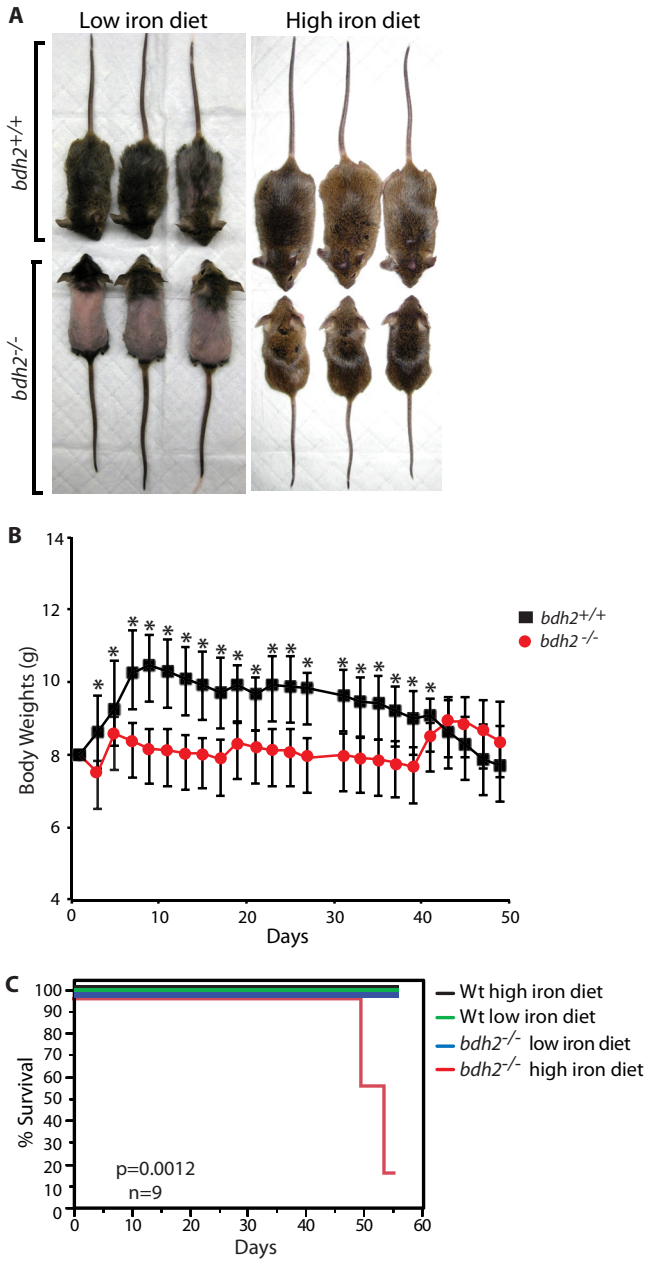

FIG 6 Iron challenge adversely affects the growth of *bdh2* null mice. (A) Morphological features of mice on low-iron and high-iron diets. (B) Growth parameters of control and *bdh2* null mice placed on a high-iron diet. (C) Survival analysis of control and *bdh2* null mice on a high-iron diet.

low-iron diet caused a decrease in iron content in the spleens of both wt and *bdh2* null mice (Fig. 7C and F). Collectively, the iron imbalance observed in *bdh2* null mice is likely to adversely affect organ function.

Supplementation with 2,5-DHBA alleviates iron overload. We previously showed that 2,5-DHBA protects cells from iron toxicity by sequestering iron (18). Additionally, *bdh2* null mice display iron overload in spleen. If the basis for iron accumulation in spleen is indeed lack of 2,5-DHBA, then supplementation with 2,5-DHBA should correct this defect. To examine this hypothesis, we injected 12-week-old control or *bdh2* null mice with 500 mg/kg 2,5-DHBA split into two doses, and each dose was injected intraperitoneally 24 h apart. Mice were sacrificed 24 h after last injection of 2,5-DHBA, and iron levels in the blood and tissues of these mice were determined. Injection with vehicle used to solubilize 2,5-DHBA had no effect on serum iron parameters in both control and *bdh2* null mice (Fig. 8A and B). In contrast, injection of 2,5-DHBA lowered serum iron levels as well as serum Tf iron saturation in *bdh2* null mice (Fig. 8A and B). Injection of 2,5-DHBA into control mice also lowered serum iron and serum Tf iron saturation (Fig. 8A and B).

Finally, we assessed iron levels in spleen samples from control or *bdh2* null mice injected with 2,5-DHBA or vehicle. Iron content in the spleen of *bdh2* null mice was higher than that in control mice (Fig. 8C and D). Injection of 2,5-DHBA reduced the iron content of the spleen in these mice as determined by histological and quantitative analyses (Fig. 8C and D). Combined, these results suggest that 2,5-DHBA supplementation reduces iron overload in the spleen.

Disruption of *bdh2* does not alter ketone body metabolism. We next sought to determine the biological significance of BDH2 deficiency *in vivo*. An earlier study suggested a role for BDH2 in ketone body metabolism. Based on computational modeling, it was proposed that BDH2 binds to and oxidizes cytosolic ketone bodies (28, 39). However, whether BDH2 has a significant role in ketone body metabolism *in vivo* has not been demonstrated. Therefore, we evaluated levels of ketone bodies in plasma samples obtained from wt and *bdh2* null mice, specifically D-β-OH butyric acid, the most abundant ketone in the body. As expected, wt mice displayed basal levels of D-β-OH butyric acid (Fig. 9A). Interestingly, measurement of D-β-OH butyrate in *bdh2* null mice yielded levels comparable to that of wt mice (Fig. 9A) (22). Additionally, evaluation of acetoacetate also suggested no ketoacidosis in *bdh2* null mice (Fig. 9B) (22). In mammals, ketone bodies are derived from the oxidation of fatty acids, which are then exported to other tissues to be used as fuel (40). Defects in ketone body oxidation result in ketosis and channeling of ketone bodies via coenzyme A (CoA) transferase to form fatty acids. Therefore, we next assessed cholesterol, free fatty acid (FFA), and triglyceride levels in plasma samples from wt and *bdh2* null mice. Plasma fatty acid measurements in *bdh2* null mice are similar to the levels found in wt mice (22). Thus, multiple lines of evidence suggest that BDH2 deficiency does not impair ketone body metabolism, counter to the computational model's prediction.

DISCUSSION

We previously showed that depleting the siderophore by inhibiting expression of *bdh2* in yeast and zebrafish embryos results in mitochondrial iron deficiency and, as a consequence, decreased heme biosynthesis (18). In this report, we analyzed the origin of the anemia in *bdh2* null mice. The presence of microcytic and hypochromic anemia in *bdh2* null mice, as noted by decreased MCV and MCHC, suggests defects in iron acquisition or availability or heme. Additionally, absence of BDH2 leads to abnormal accumulation of iron in the spleen and, to a lesser extent, the liver. Lower serum iron and higher tissue iron in *bdh2* null mice are reminiscent of anemia of chronic inflammation. Accumulation of iron in spleen and liver in *bdh2* null mice raises the possibility that BDH2 affects iron export (described below).

Members of the SDR family of proteins are implicated in disparate cellular processes (39). Based on a computational design,

TABLE 1 Hematologic parameters of wt and *bdh2* null mice on normal and iron-manipulated diets

Parameter[a]	Result (mean ± SD) for[b]:								
	Low-iron diet			High-iron diet			Basal-iron diet		
	wt ($n = 6$)	$bdh2^{-/-}$ ($n = 5$)	P	wt ($n = 10$)	$bdh2^{-/-}$ ($n = 9$)	P	wt ($n = 5$)	$bdh2^{-/-}$ ($n = 5$)	P
WBCs ($10^3/\mu l$)	10.7 ± 3.3	9.5 ± 3	>0.05	3.79 ± 2.5	4.1 ± 1.9	>0.05	11.1 ± 6	11.5 ± 2.1	>0.05
RBCs ($10^6/\mu l$)	7.06 ± 1.9	7.11 ± 3	>0.05	2.62 ± 1.4	3.64 ± 2.2	>0.05	10.4 ± 1.2	12.3 ± 0.7	<0.05
Hemoglobin (g/dl)	7.48 ± 2.9	6.18 ± 3.5	>0.05	4.63 ± 2.6	5.58 ± 3.5	0.05	16.6 ± 1.55	14.6 ± 1.6	>0.05
HCT (%)	24.2 ± 6	29.2 ± 12	>0.05	14.1 ± 8.3	17.64 ± 11	0.02	47.7 ± 4.3	55.4 ± 10	>0.05
MCV (fl)	38.1 ± 8	41.2 ± 7.4	0.001	52.2 ± 9.7	47.1 ± 3.8	0.04	53.4 ± 7.8	46 ± 2	<0.05
MCH (g/dl)	10.6 ± 2	11.4 ± 1.8	>0.05	17.3 ± 3.1	15.1 ± 0.65	0.03	15.9 ± 0.56	16.5 ± 3.5	>0.05
MCHC (g/dl)	28.6 ± 2	27.7 ± 2.22	>0.05	33.2 ± 2.7	32.2 ± 1.48	>0.05	34.8 ± 0.86	31.2 ± 0.7	<0.05
RDW (%)	27.3 ± 1.1	28.8 ± 2	>0.05	23 ± 4	20 ± 1.19	>0.05	6.83 ± 0.75	8.65 ± 1	>0.05
Platelets ($10^3/\mu l$)	1,028 ± 306	942 ± 341	>0.05	1,403 ± 1,210	2,068 ± 1,048	>0.05	754 ± 396	594 ± 247	>0.05

[a] WBCs, white blood cells; RBCs, red blood cell; HCT, hematocrit; MCV, mean corpuscular volume; MCH, mean corpuscular hemoglobin; RDW, red cell distribution width.
[b] Statistical differences were calculated by two-tailed Student's *t* test.

BDH2 was proposed to bind and oxidize ketone bodies in the cytoplasm (28, 39). We created mice lacking BDH2; specifically we deleted exon 7 in *bdh2*, which encodes the catalytic site of BDH2 (18, 22). Amino acid residues encoded by exon 7 of *bdh2* form a helix, which is located at a dimer interface within the tetramer (2 of these helices in 2 adjacent monomers interact with each other in the tetramer) (28). Removal of the helices prevents proper dimer/tetramer formation. Removal of this helix also prevents the monomer from folding properly. Additionally, within this helical stretch of residues are 3 amino acids that form the active site: Tyr147 and Lys151 interact with the bound NAD (cofactor), and Arg144 interacts with a sulfate in the active site (28). Thus, removal of exon 7 results in abrogation of the enzymatic activity of BDH2 and also destabilizes the structure of BDH2.

Many lines of evidence suggest that BDH2 may be dispensable for oxidation of ketone bodies. First, we found that BDH2 deficiency does not alter ketone body levels. Second, cytosolic BDH2 is only 20% identical to BDH1, a mitochondrial enzyme involved in NAD^+/NADPH-dependent oxidation/reduction of ketone bodies (40). Last, the majority of ketone bodies are ferried into mitochondria (40) to fuel energy reactions. Therefore, the contribution of cytosolic ketone oxidation mediated by BDH2 is minimal.

One of the least understood aspects of cellular iron metabolism is the trafficking of iron within the cell (4, 5). Iron is generally believed to be taken up by the cell via the Tf pathway and then routed to mitochondria through the cytoplasm. The facilitators of cytosolic iron trafficking to mitochondria remain enigmatic. Previously, we showed that BDH2 or DHRS6, a member of the short-chain dehydrogenases, catalyzes 2,5-DHBA biosynthesis (18). We also found that 2,5-DHBA, the mammalian siderophore, facilitates mitochondrial iron uptake (18). Based on the results presented in this report, as well as in our recent paper (22), we suggest that cytosolic BDH2 is important for 2,5-DHBA biosynthesis and cellular iron metabolism in mammals for the following reasons. First, mammalian BDH2 is highly homologous to bacterial EntA (over 45% similarity and ~31% identical) (18), which oxidizes 2,3-dihydro-2,3-DHBA to 2,3-DHBA. Therefore, based on the high degree of homology, the major function of BDH2 is likely to be in DHBA biosynthesis. Second, in agreement with the above-mentioned prediction, we showed that the absence of BDH2 abrogates 2,5-DHBA biosynthesis both *in vivo* and in cultured cells (18; this report). Third, contrary to the purported function based on a computational study (28), ketone body levels are unchanged in *bdh2* null mice. Fourth, *bdh2* is the only member of the SDR family that contains an iron response element (IRE) and is regulated by iron in human and primate cells (41). The presence of an IRE further reinforces the hypothesis that *bdh2* plays a role in iron metabolism in human and primate cells. *bdh2* was found to be increased in sodium/hydrogen exchanger NHA2-deficient cells (42). Tf receptor endocytosis in *NHA2* null pancreatic β cells is significantly reduced (42). Thus, it was proposed that an increase in *bdh2* may be a mechanism to maintain iron homeostasis in β cells (42). Absence of BDH2 results in alterations in cellular iron metabolism both *in vivo* as well as in cell culture models (see reference 17 and this report). Finally, supplementation with 2,5-DHBA partially rescued iron accumulation in *bdh2* null mice. Combined, all of these results strongly support a role for BDH2/2,5-DHBA in cellular iron metabolism.

A recent report suggested that 2,5-DHBA does not bind iron in the cell (43). This study did not take into consideration, and failed to cite, many important studies that support our conclusions. (i) For instance, interaction of 2,5-DHBA (gentisic acid) with iron is known (44). (ii) In addition, the conclusions of Correnti et al. regarding the inability of 2,5-DHBA to bind ferric iron contradict a known interaction between maduraferrin and iron (45). The structure of maduraferrin demonstrates that 2,5-DHBA does bind in a bidentate fashion to iron (45). This supports the conclusions of an earlier study (44). However, it is also possible that hydroxamate and acid hydrazide moieties contribute to additional iron affinity of maduraferrin (45). (iii) Finally, in contrast to the study by Correnti et al., results from our laboratory as well as others have reported interaction of 24p3 with 24p3R (46–48). Thus, noninclusion of these reports that would otherwise support our conclusions makes it difficult to interpret the observations of Correnti et al. Nonetheless, in light of their study, we extensively studied the complex formation of ferric iron salts with 2,5-DHBA in pH ranges of 2.5 to 9.0 at 298.15 K in water as a solvent using kinetic and equilibrium UV spectroscopy. We found that complexation with Fe(III) and 2,5-DHBA occurs at a 1:3 ratio, which was confirmed by high-resolution mass spectrometry. Based on these results, we propose that 2,5-DHBA binds to ferric iron ion via the salicylate mode (S. Porwal, E. Furia, M. E. Harris, R. Viswanathan, and L. Devireddy, submitted for publication).

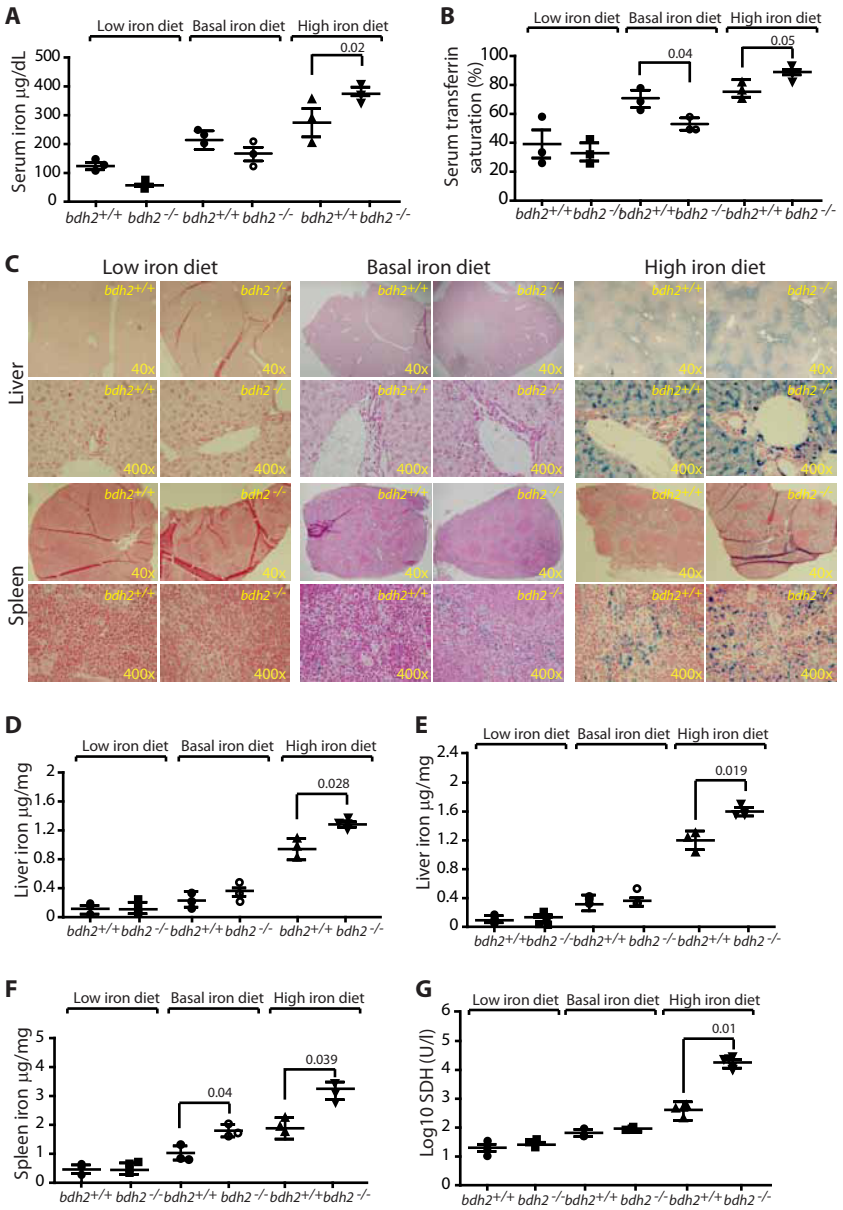

FIG 7 Iron parameters in control and *bdh2* null mice fed with iron-manipulated diets. (A and B) Serum iron indices in control and *bdh2* null mice placed on a low-iron diet, basal-iron diet, and high-iron diet. Serum iron and transferrin saturation were measured in nonhemolyzed sera of control and *bdh2* null mice. Data are presented as means ± SD. (C) Perls Prussian blue staining to detect tissue iron in liver and spleen sections from control and *bdh2* null mice fed with a low-iron diet, basal-iron diet, and high-iron diet. Nonheme iron stains blue. Representative images from specimens collected from at least 3 mice per genotype are shown. (D) Quantitative determination of liver iron content (μg/mg of wet tissue weight) of control and *bdh2* null mice placed on a low-iron diet, basal-iron diet, and high-iron diet by colorimetry. At least 3 mice per time point and genotype were analyzed. Data are presented as means ± SD. (E) Atomic absorption spectroscopy analysis of liver iron content (μg/mg of tissue wet weight) in control and *bdh2* null mice placed on a low-iron diet, basal-iron diet, and high-iron diet. At least 3 mice per time point and genotype were analyzed. Data are presented as means ± SD. (F) Quantitative determination of tissue iron content (μg/mg of wet tissue weight) in spleen from control and *bdh2* null mice placed on a low-iron diet, basal-iron diet, and high-iron diet. At least 3 mice per time point and genotype were analyzed. Data are presented as means ± SD. (G) SDH levels in sera from control and *bdh2* null mice fed with a low-iron diet, basal-iron diet, and high-iron diet. Enzyme levels are indicated in logarithmic scale. At least 3 mice per time point and genotype were analyzed. Data are presented as means ± SD.

Correnti et al. fail to convincingly demonstrate steric hindrance between iron-bound 2,5-DHBA and the binding pocket of 24p3. Correnti et al. rely on a structural model to show that steric hindrance "precludes binding" of iron-bound 2,5 DHBA to 24p3. However, the reported model allows no flexibility in the position of any residues comprising the 24p3 binding site or any shift in the modeled 2,5-DHBA position or orientation to resolve the exhibited clash. Such a model is unrealistic. Indeed, it is well known that receptor-ligand interactions often involve movement of binding site residues (49). Additionally, published structures of 24p3 bound to various ligands show that the complexes exhibit side-chain flexibility and ligand movement (50).

We found that by 12 weeks of age, *bdh2* null mice accumulate significant amounts of iron, especially in the spleen and, to a lesser

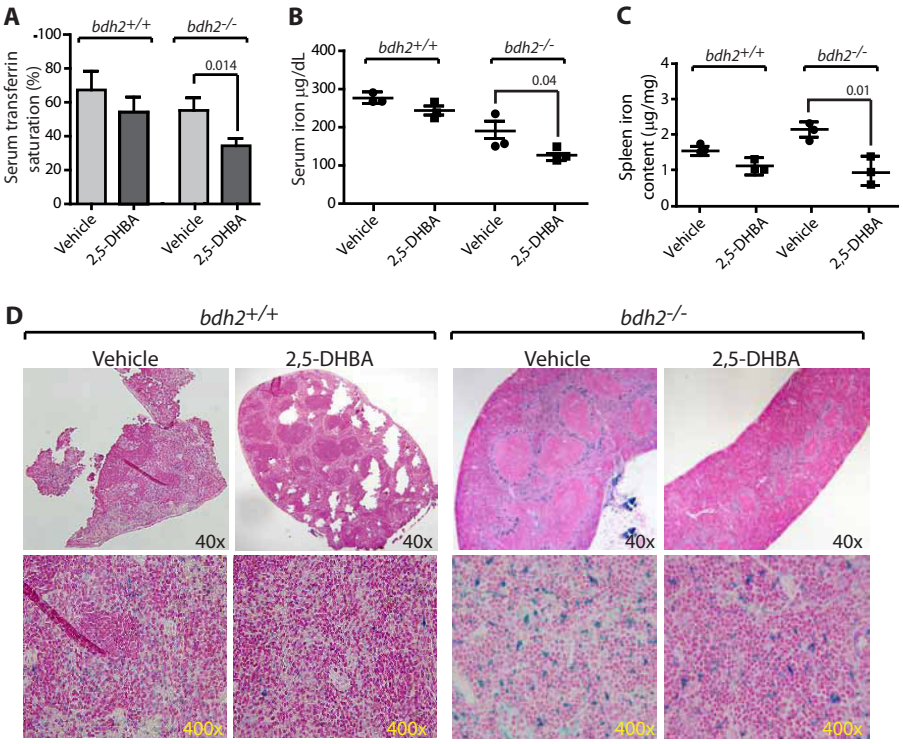

FIG 8 Supplementation with 2,5-DHBA alleviates iron overload in *bdh2* null mice. (A and B) Serum iron indices in control and *bdh2* null mice in *bdh2* null mice injected with vehicle or 2,5-DHBA. Serum iron and transferrin saturation were measured in nonhemolyzed sera of wt or *bdh2* null mice injected with vehicle or 2,5-DHBA. Data are presented as means ± SD. (C) Quantitative determination of tissue iron content (μg/mg of tissue wet weight) in spleen of control or *bdh2* null mice injected with vehicle or 2,5-DHBA. At least 3 mice per treatment condition were analyzed. Data are presented as means ± SD. (D) Histological detection of tissue iron in spleen sections from control or *bdh2* null mice injected with vehicle control of 2,5-DHBA by Perls staining. Blue staining represents iron accumulation in cells. Representative images from specimens collected from at least 3 mice per treatment condition are shown.

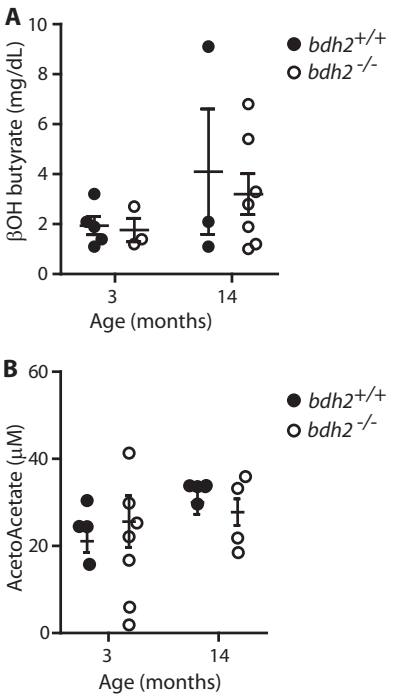

FIG 9 Bdh2 deficiency does not alter ketone body metabolism. (A and B) Measurement of D-β-OH butyric acid and acetoacetate levels in plasma of 8-week-old female wt and *bdh2* null mice. Data are presented as means ± SD.

extent, in the liver. In contrast, the tissue iron content in spleen is unremarkable in geriatric mice. Thus, it appears that over time these mice develop compensatory mechanisms to prevent iron accumulation in the spleen. We also found that dietary iron content influences the phenotype of *bdh2* null mice. *bdh2* null mice placed on a high-iron diet gain weight slowly and are much smaller than wt mice placed on the same diet. Furthermore, a high-iron diet causes the demise of *bdh2* null mice, presumably the consequence of iron-induced toxicity. Siderophore-depleted cells contain higher levels of ROS and are substantially more sensitive to oxidative stress (18). Chelated iron is much less reactive than free iron in generating ROS. Therefore, by sequestering free iron, 2,5-DHBA protects cells from oxidative stress (18) or by scavenging free radicals (51).

An increase in the ZnPP/H ratio suggests a defect in iron metabolism, perhaps resulting from a defect in iron utilization, systemic iron deficiency, or defects in recycling of senescent RBCs (31, 32). Macrophages recycle heme from senescent RBCs and store iron in ferritin, which is directed to the lysosomal pathway to meet the demands of iron need. Ferroportin regulates iron egress from macrophages into circulation (52). Free heme is very toxic, and lack of the antioxidant enzyme BDH2 (18, 51) leads to a nonenzymatic destruction of heme, forcing iron to depart from its physiological path toward ferroportin. Therefore, BDH2 deficiency impairs the recycling of hemoglobin iron by macrophages. This scenario also explains iron accumulation and an increase in the ZnPP/H ratio in *bdh2* null mice.

In contrast to the phenotype of *bdh2* null mice on a high-iron diet, iron deficiency resulted in extreme anemia. Significantly, we found severe alopecia in *bdh2* null mice that were maintained on a low-iron diet. However, these results (high iron in liver/spleen and low serum iron) are similar to anemia of chronic disease (a.k.a., anemia of inflammation) in which iron stores are increased in these tissues and are prevented from being exported. Thus, BDH2 may affect iron export from cells and not intracellular import.

Our previous studies showed that siderophore depletion results in iron-deficient mitochondria. We also found that mitochondrial iron deficiency resulting from siderophore depletion leads to mitochondrial stress and promotes mitophagic clearance of mitochondria (Z. Liu and L. Devireddy, unpublished data). Mitochondria influence nuclear gene expression via a poorly understood retrograde signaling pathway (53). Thus, loss of mitochondria in siderophore-depleted cells may in part explain the altered nuclear transcriptome observed in spleen samples from *bdh2* null mice. Alternatively, alterations in the cellular LIP might affect the nuclear LIP leading to altered transcription.

In summary, the current findings reveal an important role for BDH2 in cellular iron metabolism while demonstrating that basal levels of ketone bodies in *bdh2* null mice are indistinguishable from those of wt mice.

ACKNOWLEDGMENTS

We thank Barry Paw for providing protocols, Alan Tartakoff, Robert B. Petersen, and Dave Goetz for editorial assistance, Gangarao Davuluri for help with mouse experimentation, and Vivian Yee and Vijay Kumar for expert advice on the structure of mutant BDH2. We also thank anonymous reviewer 2 for suggestions that significantly improved the manuscript.

This work is supported by K01CA113838, R01DK081395, and Case Western Reserve University startup funds to L.D. L.D. is also a recipient of career developmental awards from the March of Dimes and American Society of Hematology.

REFERENCES

1. **Hattangadi S, Wong P, Zhang L, Flygare J, Lodish HF.** 2011. From stem cell to red cell: regulation of erythropoiesis at multiple levels by multiple proteins, RNAs and chromatin modifications. Blood **118:**6258–6268. http://dx.doi.org/10.1182/blood-2011-07-356006.
2. **Orkin SH, Zon LI.** 2008. Hematopoiesis: an evolving paradigm for stem cell biology. Cell **132:**631–644. http://dx.doi.org/10.1016/j.cell.2008.01.025.
3. **Petrak J, Myslivcova D, Man P, Cmejlova J, Cmejla R, Vyoral D.** 2007. Proteomic analysis of erythroid differentiation induced by hexamethylene bisacetamide in murine erythroleukemia cells. Exp. Hematol. **35:**193–202. http://dx.doi.org/10.1016/j.exphem.2006.10.007.
4. **Richardson DR, Lane DJ, Becker EM, Huang ML, Whitnall M, Rahmanto YS, Sheftel AD, Ponka P.** 2010. Mitochondrial iron trafficking and the integration of iron metabolism between the mitochondrion and cytosol. Proc. Natl. Acad. Sci. U. S. A. **107:**10775–10782. http://dx.doi.org/10.1073/pnas.0912925107.
5. **Napier I, Ponka P, Richardson DR.** 2005. Iron trafficking in the mitochondrion: novel pathways revealed by disease. Blood **105:**1867–1874. http://dx.doi.org/10.1182/blood-2004-10-3856.
6. **Meneghini R.** 1997. Iron homeostasis, oxidative stress, and DNA damage. Free Radic. Biol. Med. **23:**783–792. http://dx.doi.org/10.1016/S0891-5849(97)00016-6.
7. **Shaw GC, Cope JJ, Li L, Corson K, Hersey C, Ackerman GE, Gwynn B, Lambert AJ, Wingert RA, Traver D, Trede NS, Barut BA, Zhou Y, Minet E, Donovan A, Brownlie A, Balzan R, Weiss MJ, Peters LL, Kaplan J, Zon LI, Paw BH.** 2006. Mitoferrin is essential for erythroid iron assimilation. Nature **440:**96–100. http://dx.doi.org/10.1038/nature04512.
8. **Chen W, Paradkar PN, Li L, Pierce EL, Langer NB, Takahasi-Makise N, Hyde BB, Shirihai OS, Ward DM, Kaplan J, Paw BH.** 2009. Abcb10 physically interacts with mitoferrin-1 (Slc25a37) to enhance its stability and function in the erythroid mitochondria. Proc. Natl. Acad. Sci. U. S. A. **106:**16263–16268. http://dx.doi.org/10.1073/pnas.0904519106.
9. **Ajioka RS, Phillips JD, Kushner JP.** 2006. Biosynthesis of heme in mammals. Biochim. Biophys. Acta **1763:**723–726. http://dx.doi.org/10.1016/j.bbamcr.2006.05.005.
10. **Wang J, Pantopoulos K.** 2011. Regulation of cellular iron metabolism. Biochem. J. **434:**365–381. http://dx.doi.org/10.1042/BJ20101825.
11. **Pantopoulos K, Porwal S, Tartakoff A, Devireddy LR.** 2012. Mechanisms of mammalian iron homeostasis. Biochemistry **51:**5705–5724. http://dx.doi.org/10.1021/bi300752r.
12. **Glickstein H, Ben El R, Shvartsman M, Cabantchik ZI.** 2005. Intracellular labile iron pool as direct targets of iron chelators: a fluorescence study of chelator action in living cells. Blood **106:**3242–3250. http://dx.doi.org/10.1182/blood-2005-02-0460.
13. **Kruszewski M.** 2003. Labile iron pool: the main determinant of cellular response to oxidative stress. Mutat. Res. **531:**81–92. http://dx.doi.org/10.1016/j.mrfmmm.2003.08.004.
14. **Kakhlon O, Cabantchik ZI.** 2002. The labile iron pool: characterization, measurement, and participation in cellular processes. Free Radic. Biol. Med. **33:**1037–1046. http://dx.doi.org/10.1016/S0891-5849(02)01006-7.
15. **Nielands JB.** 1995. Siderophores: structure and functions of microbial iron transport compounds. J. Biol. Chem. **27:**26723–26726.
16. **Fernandez-Pol JA.** 1978. Isolation and characterization of a siderophore-like growth factor from mutants of SV40-transformed cells adapted to picolinic acid. Cell **14:**489–499. http://dx.doi.org/10.1016/0092-8674(78)90235-0.
17. **Jones R, Peterson C, Grady R, Cerami A.** 1980. Low molecular weight iron-binding factor from mammalian tissue that potentiates bacterial growth. J. Exp. Med. **151:**418–428. http://dx.doi.org/10.1084/jem.151.2.418.
18. **Devireddy LR, Hart DO, Goetz DH, Green MR.** 2010. A mammalian siderophore synthesized by an enzyme with a bacterial homolog involved in enterobactin production. Cell **141:**1006–1017. http://dx.doi.org/10.1016/j.cell.2010.04.040.
19. **Crosa JH, Walsh CT.** 2002. Genetics and assembly line enzymology of siderophore biosynthesis in bacteria. Microbiol. Mol. Biol. Rev. **66:**223–249. http://dx.doi.org/10.1128/MMBR.66.2.223-249.2002.
20. **Franke D, Lorbach V, Esser S, Dose C, Sprenger GA, Halfar M, Thommes J, Muller R, Takors R, Muller M.** 2003. (*S*,*S*)-2,3-Dihydroxy-2,3-dihydroxy benzoic acid: microbial access with engineered cells of Escherichia coli and application as starting material in natural-product synthesis. Chem. Eur. J. **9:**4188–4196. http://dx.doi.org/10.1002/chem.200204265.
21. **Zhang AS, Sheftel AD, Ponka P.** 2005. Intracellular kinetics of iron in reticulocytes: evidence for endosome involvement in iron targeting to mitochondria. Blood **105:**368–375. http://dx.doi.org/10.1182/blood-2004-06-2226.
22. **Liu Z, Reba S, Chen W-D, Porwal SK, Boom WH, Petersen R, Rojas R, Viswanathan R, Devireddy L.** Regulation of mammalian siderophore 2,5-DHBA in the innate immune response to infection. J. Exp. Med., in press.
23. **Blohowiak SE, Chen ME, Repyak KS, Baumann-Blackmore NL, Carlton DP, Georgieff MK, Crenshaw TD, Kling PJ.** 2008. Reticulocyte enrichment of zinc protoporphyrin/heme discriminates impaired iron supply during early development. Pediatr. Res. **64:**63–67. http://dx.doi.org/10.1203/PDR.0b013e31817328e5.
24. **Sturrock A, Alexander J, Lamb J, Craven CM, Kaplan J.** 1990. Characterization of a transferrin-independent uptake system for iron in HeLa cells. J. Biol. Chem. **265:**3139–3145.
25. **Hawley RG, Hawley TS, Cantor AB.** 2008. TLX1 (HOX11) immortalization of embryonic stem cell-derived and primary murine hematopoietic progenitors. Curr. Protoc. Stem Cell Biol. Chapter 1:Unit 1F.7. http://dx.doi.org/10.1002/9780470151808.sc01f07s7.
26. **Riemer J, Hoepken HH, Czerwinska H, Robinson SR, Dringen R.** 2004. Colorimetric ferrozine-based assay for the quantification of iron in cultured cells. Anal. Biochem. **331:**370–375. http://dx.doi.org/10.1016/j.ab.2004.03.049.
27. **Kerner J, Distler AM, Minkler P, Parland W, Peterman SM, Hoppel CL.** 2004. Phosphorylation of rat liver mitochondrial carnitine palmitoyltransferase-I effect on the kinetic properties of the enzyme. J. Biol. Chem. **279:**41104–41113. http://dx.doi.org/10.1074/jbc.M406570200.

28. **Guo K, Lukacik P, Papagrigoriou E, Meier M, Lee WH, Adamski J, Oppermann U.** 2006. Characterization of human DHRS6, an orphan short chain dehydrogenase/reductase enzyme: a novel, cytosolic type 2 R-beta-hydroxybutyrate dehydrogenase. J. Biol. Chem. **281:**10291–10297. http://dx.doi.org/10.1074/jbc.M511346200.
29. **Kim PM, Wells PG.** 1996. Phenytoin-initiated hydroxyl radical formation: characterization by enhanced salicylate hydroxylation. Mol. Pharmacol. **49:**172–181.
30. **Lolascon A, De Falco L, Beaumont C.** 2009. Molecular basis of inherited microcytic anemia due to defects in iron acquisition or heme synthesis. Hematologica **94:**395–408. http://dx.doi.org/10.3324/haematol.13619.
31. **Tian M, Campagna DR, Woodward LS, Justice MJ, Fleming MD.** 2008. *hem6*: an ENU-induced recessive hypochromic microcytic anemia mutation in the mouse. Blood **112:**4308–4313. http://dx.doi.org/10.1182/blood-2007-09-111500.
32. **Ohgami R, Campagna DR, Antiochos B, Wood EB, Sharp JJ, Barker JE, Fleming MD.** 2005. Nm1054: a spontaneous, recessive, hypochromic, microcytic anemia mutation in the mouse. Blood **106:**3625–3631. http://dx.doi.org/10.1182/blood-2005-01-0379.
33. **Ganz T, Nemeth E.** 2012. Hepcidin and iron homeostasis. Biochim. Biophys. Acta **1823:**1434–1443. http://dx.doi.org/10.1016/j.bbamcr.2012.01.014.
34. **Nemeth E, Tuttle MS, Powelson J, Vaughn MB, Donovan A, Ward DM, Ganz T, Kaplan J.** 2004. Hepcidin regulates cellular iron efflux by binding to ferroportin and inducing its internalization. Science **306:**2090–2093. http://dx.doi.org/10.1126/science.1104742.
35. **De Domenico I, Ward DM, Langelier C, Vaughn MB, Nemeth E, Sundquist WI, Ganz T, Musci G, Kaplan J.** 2007. The molecular mechanism of hepcidin-mediated ferroportin down-regulation. Mol. Biol. Cell **18:**2569–2578. http://dx.doi.org/10.1091/mbc.E07-01-0060.
36. **Labbe R, Vreman H, Stevenson D.** 1999. Zinc protoporphyrin: a metabolite with a mission. Clin. Chem. **45:**2060–2072.
37. **Lesbordes-Brion J-C, Viatte L, Bennoun M, Lou D-Q, Ramey G, Houbron C, Hamard G, Kahn A, Vaulont S.** 2006. Targeted disruption of the hepcidin 1 gene results in severe hemochromatosis. Blood **108:**1402–1405. http://dx.doi.org/10.1182/blood-2006-02-003376.
38. **Bain PJ.** 2011. Liver, p 211–230. *In* Latimer KS (ed), Duncan & Prasse's veterinary laboratory medicine clinical pathology, 5th ed. Wiley-Blackwell, West Sussex, United Kingdom.
39. **Oppermann U, Filling C, Hult M, Shafqat N, Wu X, Lindh M, Shafqat J, Nordling E, Kallberg Y, Persson B, Jornvall H.** 2003. Short-chain dehydrogenases/reductases (SDR): the 2002 update. Chem. Biol. Interact. **143–144:**247–253. http://dx.doi.org/10.1016/S0009-2797(02)00164-3.
40. **Cotter DG, Schugar RC, Crawford PA.** 2013. Ketone body metabolism and cardiovascular disease. Am. J. Physiol. Heart Circ. Physiol. **304:**H1060–H1076. http://dx.doi.org/10.1152/ajpheart.00646.2012.
41. **Liu Z, Lanford R, Mueller S, Gerhard G, Luscieti S, Sanchez M, Devireddy LR.** 2012. Siderophore-mediated iron trafficking in humans is regulated by iron. J. Mol. Med. **90:**1209–1221. http://dx.doi.org/10.1007/s00109-012-0899-7.
42. **Deisl C, Simonin A, Anderegg M, Albano G, Kovacs G, Ackermann D, Moch H, Dolci W, Thorens B, Hedgier MA, Fuster D.** 2013. Sodium/hydrogen exchanger NHA2 is critical for insulin secretion in β-cells. Proc. Natl. Acad. Sci. U. S. A. **110:**10004–10009. http://dx.doi.org/10.1073/pnas.1220009110.
43. **Correnti C, Richardson V, Sia AK, Bandaranayake AD, Ruiz M, Rahmanto YS, Kovacevic Z, Clifton MC, Holmes MA, Kaiser BK, Barasch J, Raymond KN, Richardson DR, Strong RK.** 2012. Siderocalin/Lcn2/NGAL/24p3 does not drive apoptosis through gentisic acid mediated iron withdrawal in hematopoietic cell lines. PLoS One **7:**e43696. http://dx.doi.org/10.1371/journal.pone.0043696.
44. **Wagner JG.** 1953. A study of the iron-gentisate reaction and its application. J. Am. Pharm. Assoc. **42:**104–106.
45. **Keller-Schierlein W, Hagmann Zahner H, Huhn W.** 1988. Maduraferrin, a novel siderophore from *Acinomadura madurae*. Helv. Chim. Acta **71:**1528–1534. http://dx.doi.org/10.1002/hlca.19880710619.
46. **Schroll A, Eller J, Feistritzer C, Nairz M, Sonnweber T, Moser PA, Rosenkranz AR, Theurl I, Weiss G.** 2012. Lipocalin-2 ameliorates granulocyte functionality. Eur. J. Immunol. **42:**3346–3357. http://dx.doi.org/10.1002/eji.201142351.
47. **Langelueddecke C, Roussa E, Fenton RA, Wolff NA, Lee W-K, Thévenod F.** 2012. Lipocalin-2 (24p3/neutrophil gelatinase-associated lipocalin (NGAL)) receptor is expressed in distal nephron and mediates protein endocytosis. J. Biol. Chem. **287:**159–169. http://dx.doi.org/10.1074/jbc.M111.308296.
48. **Devireddy LR, Gazin C, Zhu X, Green MR.** 2005. A cell surface receptor for lipocalin 24p3 selectively mediates apoptosis and iron uptake. Cell **123:**1293–1305. http://dx.doi.org/10.1016/j.cell.2005.10.027.
49. **Najmanovich R, Kuttner J, Sobolev V, Edelman M.** 2000. Side-chain flexibility in proteins upon ligand binding. Proteins **39:**261–268. http://dx.doi.org/10.1002/(SICI)1097-0134(20000515)39:3<261::AID-PROT90>3.0.CO;2-4.
50. **Holmes MA, Paulsene W, Jide X, Ratledge C, Strong RK.** 2005. Siderocalin (24p3) also binds carboxymycobactins, potentially defending against mycobacterial infections through iron sequestration. Structure **13:**29–41. http://dx.doi.org/10.1016/j.str.2004.10.009.
51. **Joshi R, Gangabhagirathi R, Venu S, Adhikari S, Mukherjee T.** 2012. Antioxidant activity and free radical scavenging reactions of gentisic acid: *in-vitro* and pulse radiolysis studies. Free Radic. Res. **46:**11–20. http://dx.doi.org/10.3109/10715762.2011.633518.
52. **Delaby C, Pilard N, Goncalves AS, Beaumont C, Canonne-Hergaux F.** 2005. Presence of the iron exporter ferroportin at the plasma membrane of macrophages in enhanced by iron loading and down-regulated by hepcidin. Blood **106:**3979–3984. http://dx.doi.org/10.1182/blood-2005-06-2398.
53. **Liu Z, Butow RA.** 2006. Mitochondrial retrograde signaling. Annu. Rev. Genet. **40:**159–185. http://dx.doi.org/10.1146/annurev.genet.40.110405.090613.